We are IntechOpen, the world's leading publisher of Open Access books Built by scientists, for scientists

4,800
Open access books available

122,000
International authors and editors

135M
Downloads

Our authors are among the

154
Countries delivered to

TOP 1%
most cited scientists

12.2%
Contributors from top 500 universities

WEB OF SCIENCE™

Selection of our books indexed in the Book Citation Index
in Web of Science™ Core Collection (BKCI)

Interested in publishing with us?
Contact book.department@intechopen.com

Polyaniline/ZnO Nanocomposite: A Novel Adsorbent for the Removal of Cr(VI) from Aqueous Solution

Rais Ahmad

Abstract

In recent years with the rapid economic globalization, pollution by industries and agriculture has increased, which results in decrease in the quality of ground and surface water. Pollution by heavy metals has become a serious health issue worldwide due to their nonbiodegradable and persistent nature. Therefore, extensive research has been done to develop ecofriendly and effective methods for removal of heavy metals, such as chemical precipitation, ion exchange, electrodialysis, membrane filtration, and adsorption. Among these methods, adsorption is the most recognized technique for wastewater treatment due to high-removal efficiency and ease in operation without yielding harmful by-products. Recently, nanocomposites based on biopolymer-grafted synthetic adsorbent have been used in various industrial applications including wastewater treatment. Therefore, the present chapter will be devoted for the removal of toxic heavy metals from wastewater by using bionanocomposite.

Keywords: heavy metals, bionanocomposite, adsorption, desorption

1. Introduction

In today's era, the industrialization, agriculture, and domestic activities have led to a large amount of wastewater having toxic elements such as lead, mercury, cadmium, copper, arsenic, chromium, etc., and dyes which has adversely affected human lives, animal lives, and environment. Among various heavy metals, Cr(VI) is one of the most important and toxic heavy metals due to its vast applications in industries [1, 2]. In aqueous medium, two forms of chromium exist, i.e., Cr(III) and Cr(VI), and the toxicity and reactivity of both the forms mainly depend on oxidation state of the chromium [3]. In trace amounts, Cr(III) is an essential nutrient for humans and to mammals for their maintenance of normal glucose tolerance factor, lipid, and protein metabolism [4]. On the other hand, Cr(VI) is very toxic to human as well as marine life and poses serious health problems such as liver damage and pulmonary congestion and regarded as carcinogenic also [5–7].

Various conventional methods have been developed for the adsorption of Cr(VI) in wastewater, including electrochemical precipitation, ion exchange, membrane ultrafiltration, reverse osmosis, reduction, and adsorption [8–10]. Adsorption has

been widely used for the removal of chromium from contaminated groundwater out of these methods [11] due to its low initial cost and ease of operation and high efficiency to remove toxic heavy metals. This technique can be harnessed at large scale for the treatment of polluted water as it can handle fairly large flow rates, producing a high quality of water without producing notorious sludge and residual contaminants [12–14].

Conducting polymer with metal oxide has nowadays emerged as an attractive alternative for the sequestration of wastewater, as it mainly provide larger surface area for the adsorption, interfacial adhesion between the surface of nanocomposite and metal ions, it is easily tractable and cost effective. Due to large amount of amine and imine functional groups PANI has strong affinity with metal ions and can remove heavy metal contaminants from aqueous solutions effectively [15, 16]. The stability of polymer matrix can be enhanced by addition of fillers such as natural clays, metal oxide nanoparticles, etc. [17]. Zinc oxide is known to be a potential adsorbent of Cr(VI) at high temperatures as well as at low temperatures [18]. So, the incorporation of ZnO nanoparticles in the PANI matrix not only provides thermal and mechanical strength, but also improves its adsorption properties. This improvement was attributed to the increase in the number and high dispersion of active terminal OH groups of ZnO nanoparticles with amine groups of PANI.

In the present chapter, polyaniline zinc oxide nanocomposite was synthesized by oxidative free radical polymerization of aniline monomer in presence of zinc oxide nanoparticles. The material was characterized by various analytical techniques such as FT-IR, XTD, TGA-DTG, SEM, and TEM. The nanocomposite material was further explored for the removal of Cr(VI) from aqueous solution. The effects of various adsorption parameters viz. agitation time, solution pH, adsorbent dose, initial metal ion concentration, and temperature was observed and optimized by preliminary experiments.

2. Materials and methods

2.1 Chemicals

Zinc acetate and ammonium persulfate (APS) were procured from Sigma Aldrich, India. Sodium hydroxide and potassium dichromate were procured from Merck, India. Aniline monomer was procured from Fisher Scientific, India and was distilled before use. About 1000 mg L^{-1} stock solutions of were prepared by dissolving appropriate amount of metal salts in double distilled water.

2.2 Synthesis of zinc oxide nanoparticles

ZnO nanoparticles were synthesized by direct precipitation method using zinc acetate and KOH as precursors [19]. The aqueous solution (0.2 M) of zinc acetate ($Zn(CH_3COO)_2\,2H_2O$) and the solution (0.4 M) of KOH were prepared with deionized water, respectively. The KOH solution was slowly added into zinc nitrate solution at room temperature under vigorous stirring, which resulted in the formation of a white suspension. The white product was centrifuged at 5000 rpm for 20 min and washed three times with distilled water, and washed with absolute alcohol at last. The obtained product was calcined at 500°C in air atmosphere for 3 h.

2.3 Synthesis of polyaniline/ZnO nanocomposite

The material was synthesized by methods already reported elsewhere [20]. The detailed procedure is as follows: 1 g of above synthesized ZnO nanoparticles were taken in 100 ml of 0.1 M HCl solution and sonicated for 1 h at 30°C. Now, 10 ml of distilled aniline monomer taken in 400 ml of 0.1 M HCl solution was poured in the above colloidal solution of ZnO. The mixture was allowed to stir for 2 h for complete mixing at 5°C. The reaction was proceeded with the addition of 15 g of APS. The reaction was allowed to stand for 12 h at 5°C and product obtained was washed with 0.1 M HCl solution five to six times in order to remove excess amount of unreacted aniline.

2.4 Instrumentation

The FTIR spectra of the adsorbent materials were recorded with a Perkin Elmer 1800 model IR spectrophotometer operating at frequency range from 400 to 4000 cm^{-1} using KBr pallets. X-ray diffraction (XRD) patterns of the samples were obtained using Siemens D 5005 X-ray unit Cu Kα (λ = 1:5406 Å) radiation, generated at a voltage of 40 kV and a current of 40 mA was used as the X-ray source. Scanning electron microscopy and electron diffraction scattering (SEM/EDS) analysis were done using GSM 6510LV scanning electron microscope. The particle size and structure of the synthesized nanocomposite were observed by using JEM 2100 transmission electron microscope (TEM). The thermal stability was determined by derivative thermal analysis (DTG, Perkin Elmer Pyris 6) and DTA (Perkin Elmer model, STA 6000). The thermograms were recorded for 20 mg of powder sample at a heating rate of 10°C min^{-1} in the temperature range of 30–800°C under nitrogen atmosphere. The concentration of metal ions in the solution was measured by atomic absorption spectrophotometer (AAS) model GBC-902. Elico Li 120 pH meter was used to adjust the pH of the solutions.

2.5 Adsorption experiments

The adsorption experiments were performed using batch equilibrium technique in aqueous solutions in the temperature range of 30–50°C at pH 2. For this, 0.04 g of adsorbents was added to 20 ml of Cr(VI) solution of various concentrations (from 10, 50, 100 mg L^{-1}) and shaken in a thermostatic water-bath shaker operated at 120 rpm. After equilibrium was attained, the adsorbent was removed and the supernatant was collected after attaining equilibrium. The concentrations of Cr(VI) in supernatant were measured using atomic absorption spectrophotometer (AAS). The kinetic experiments were performed at three different Cr(VI) ion concentrations mainly at 10, 50, and 100 mg L^{-1} at pH 2 and 3. The effect of time on the adsorption of Cr(VI) ions on PAZO nanocomposite was studied at 10–300 min and the equilibrium was reached at 120 min. The effect of adsorbent dose and initial metal ion concentration was also studied. The amount of metal ions adsorbed onto PAZO was calculated by a mass balance relationship:

$$q_e = \frac{(C_o - C_e)V}{W} \qquad (1)$$

where q$_e$ is the amount of metal ion adsorbed per unit weight of the adsorbent (mg g^{-1}); C$_o$ and C$_e$ are the concentrations of the metal ion in the initial solution (mg L^{-1}) and after adsorption, respectively; *V* is the volume of the adsorption medium (*L*); and *W* is the amount of the adsorbent (g).

3. Results and discussion

3.1 Characterization of PAZO

3.1.1 XRD analysis

XRD analysis of bulk composite was done and it was seen that the characteristic peak of ZnO nanoparticles were obtained at 2θ values of 8.03, 11.87, 31.71, 34.38, 38.18, 47.47, 58.51, 62.77, and 68.98° given in **Figure 1** which corresponds to Miller indices (100), (002), (101), (102), (110), (103), and (201), respectively. The crystalline size calculated using Scherer formula was found to be 31 nm which is also confirmed by TEM micrograph. The PANI peak diffracted at an angle of 25.72°, respectively, in the XRD pattern showing low crystallinity for conductive polymers due to the repetition of benzenoid and quinoid rings in PANI chains. Peaks of PANI-ZnO composites shift slightly higher values of 2θ. It can be seen that the XRD patterns of nanocomposites represent the peaks from ZnO and PANI. This is because of the presence of ZnO nanoparticles which is equal to 5% and it has significant effect on diffraction pattern of PANI. According to **Figure 1**, two distinct sharp peaks at 2θ = 19.311 and 25.721 with planes of (010) and (200), respectively, are shifted negligibly but their intensity increases by the reinforcement of the ZnO nanoparticles in PANI matrix. Additionally, one peak at 2θ = 23.21 with plane of (102) appears which is related to PANI-CSA and its intensity is increased by adding ZnO nanoparticles. XRD results confirm the effect of ZnO nanoparticles in PANI-ZnO nanocomposites. **Figure 1** shows that intensity of the peaks was increased by incorporation of 5% ZnO nanoparticles, which means that there is an interaction of ZnO nanoparticles and PANI by formation of hydrogen bonding between H–N and oxygen of ZnO [21].

3.1.2 Thermal analysis

Thermal stability of PANI and PAZO was analysed by TGA and the thermograms are given in **Figure 2**. The TGA thermogram of pure PANI shows three-step
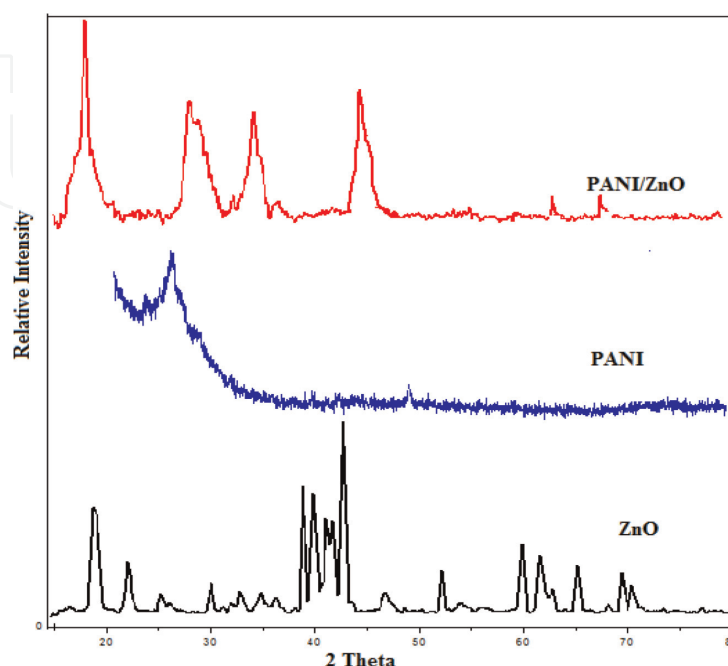

Figure 1.
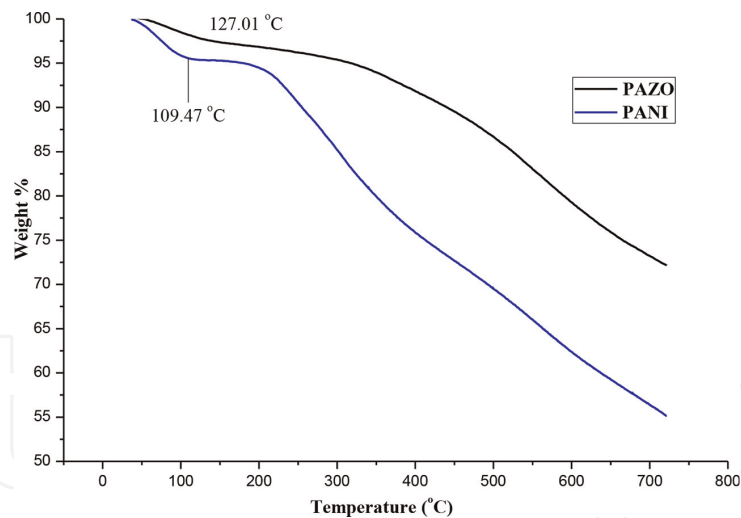*XRD spectra of ZnO, PANI and PAZO.*

Figure 2.
TGA thermograms of PANI and PAZO.

degradation of weight in the range of 30–800°C. The first weight loss of at around 109.47°C is due to evaporation of water. The second stage of weight loss starting at around 140°C up to 370°C almost 60% substance weight loss which represents the degradation of low molecular weight polymers and almost 45% weight loss for PANI was observed at 700°C [22]. From 370°C onward, degradation of PANI chains takes place up to 800°C, in which almost 90% mass loss is observed. The PAZO also shows same stages of weight loss with little bit of higher thermal stability as compare to pure PANI due to incorporation of ZnO in PANI matrix and a weight loss of 28% was observed at 800°C.

3.1.3 Surface analysis (SEM with EDX)

Morphologies of the PANI-ZnO nanocomposite with its EDX image before and after adsorption of Cr(VI) are shown in **Figure 3**. Nanocomposite reveals flaky fibrous structure shaped structure. These nanocomposites should give the opportunity to obtain improved capacitance due to surface effects. The size of the flakes and fibers decreased due to adsorption of Cr(VI). The SEM images help us to draw a conclusion that the doping of ZnO nano-rods has a strong effect on the morphology of PANI, since PANI has various structures such as granules, nanofibers, nanotubes, nanospheres, microspheres, and flakes.

3.1.4 Transmission electron microscope (TEM) analysis

Due to the low magnification in SEM micrographs, it is difficult to observe ZnO nanoparticles in the nanocomposite matrix; thus, an appropriate way for observing them in polymer matrix is by the use of TEM. According to the TEM micrographs in **Figure 4**, PANI and ZnO nanoparticles have formed a nanocomposite in which the nanoparticles are embedded in the polymer matrix. It is obvious that ZnO nanoparticles were uniformly coated by PANI. The average size of ZnO nanoparticles was observed as 31.2 nm.

3.1.5 FTIR analysis

PANI and PAZO nanocomposite were characterized by using the FTIR technique. **Figure 5** shows the FTIR pattern of ZnO nanoparticles, PANI and PAZO nanocomposite. The characteristic absorption bands of PANI are 515.71 cm^{-1}
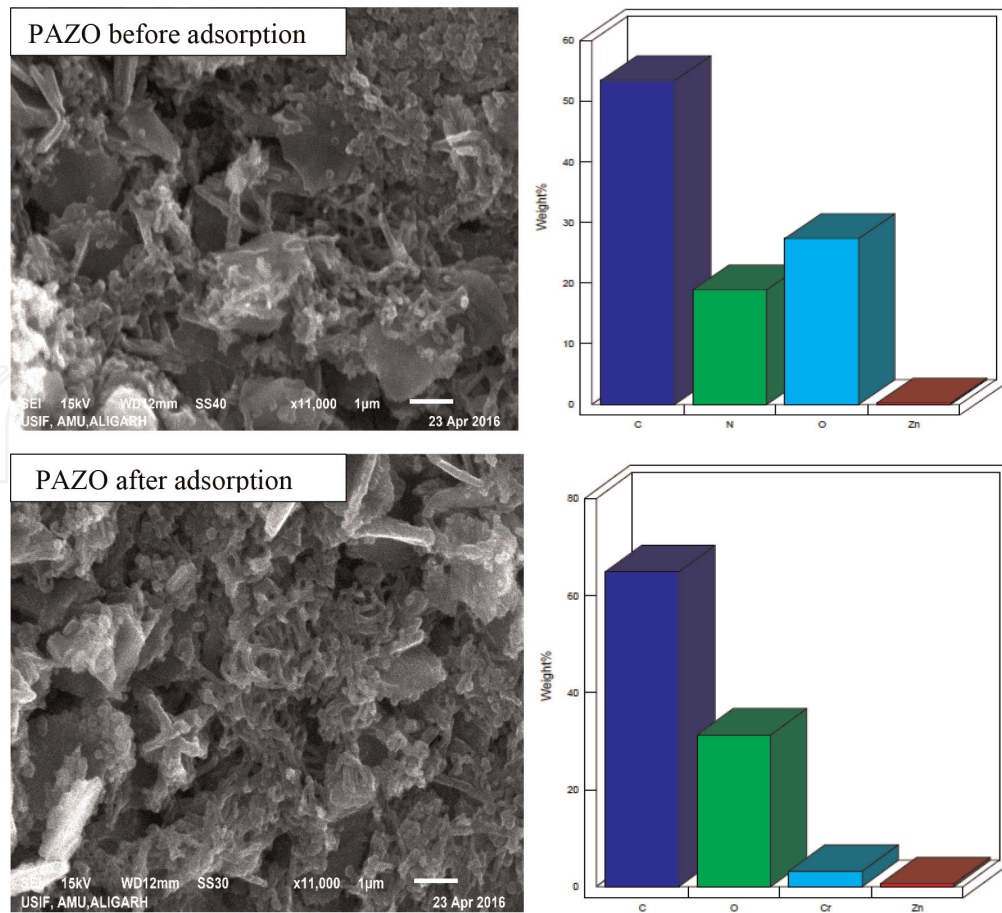
Figure 3.
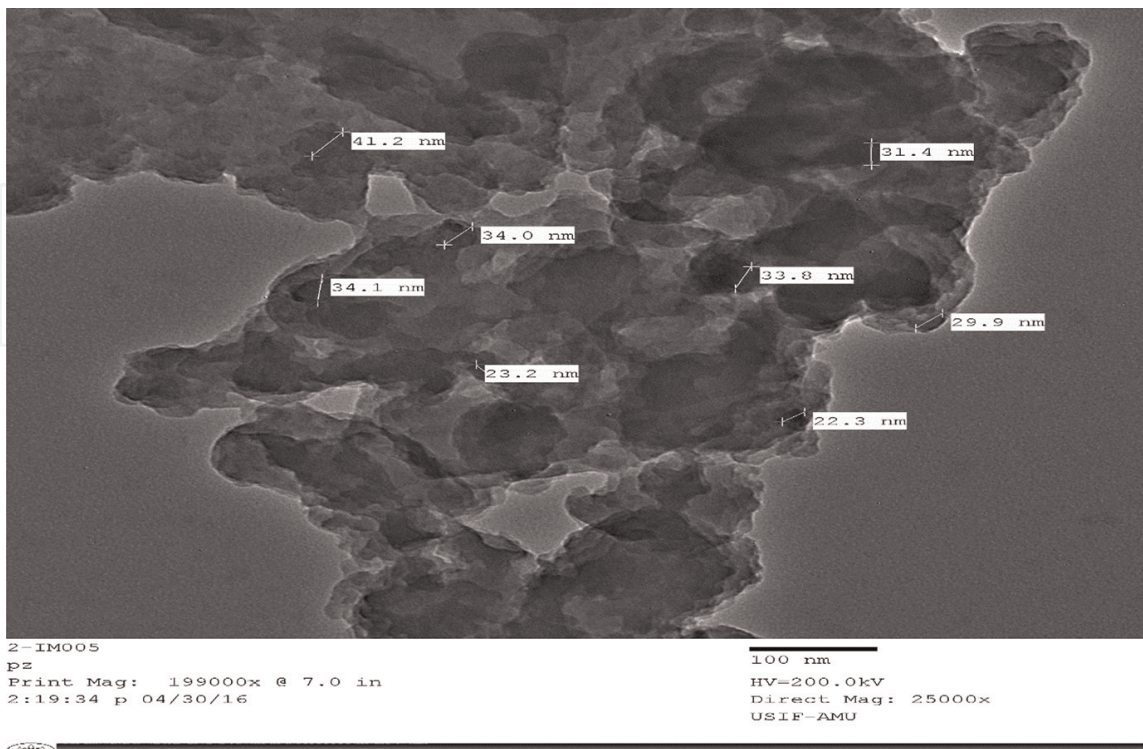*SEM images of PAZO before and after adsorption of Cr(VI) with its EDX image.*

Figure 4.
TEM image of PAZO.

(C–N–C bonding mode of aromatic ring); 592.85 and 700.84 cm^{-1} (C–C, C–H bonding mode of aromatic ring); 831.98 cm^{-1} (C–H out of plane bonding in benzenoid ring); 1040.26, 1302.53, and 1503.09 cm^{-1} (C–N stretching of benzenoid ring), and 1572.52 cm^{-1} (C–N stretching of quinoid ring). The PAZO nanocomposite shows the same characteristic peaks. However, there is an evidence of peak displacement when ZnO nanoparticles are added to the PANI. These shifts include 1572.51–1587.94, 1503.09–1510.81, 1155.97–1148.25, 1040.26–1047.97, 831.98–862.84, and 592.85–600.23 cm^{-1}. Furthermore, in PAZO nanocomposite, a broad peak appeared in 3470 cm^{-1}, which can be associated to the interaction between ZnO nanoparticles and PANI by formation of hydrogen bonding between H–N and oxygen of ZnO. So, the peak displacement that was observed in FTIR spectra may be ascribed to the formation of hydrogen bonding between ZnO and the N–H group of PANI on the surface of the ZnO nanoparticles.

3.2 Adsorption behavior of PAZO toward Cr(VI)

3.2.1 Effect of pH

One the most important parameter that directly affects the adsorption of Cr(VI) is pH of the solution. The effect of the initial solution pH on the removal of Cr(VI) was studied with 0.04 g of PAZO nanocomposite, 20 ml of 10, 50, and 100 mg L^{-1} Cr(VI) solution with different pH in the range 2–7 at 30°C. The effect of pH on
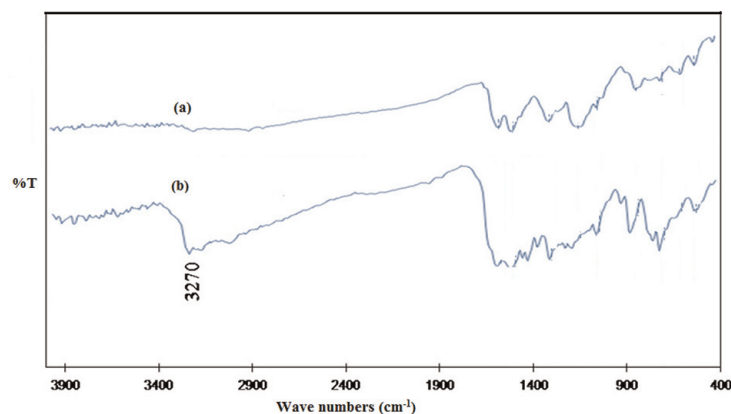

Figure 5.
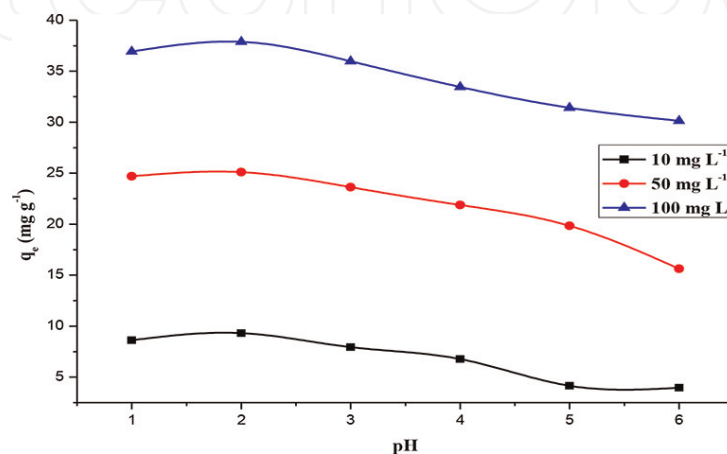*FTIR spectra of (a) PANI and (b) PAZO.*

Figure 6.
Effect of pH on adsorption of Cr(VI) on PAZO at 10, 50, and 100 mg L^{-1} initial metal ion concentrations.

sorption of Cr(VI) has been shown in **Figure 6**. It was found that the maximum adsorption capacity for Cr(VI) was in the pH value of 2 and as the pH value increases the adsorption capacity decreases. Various forms of Cr(VI) in water such as $HCrO_4^-$ in acidic medium, CrO_4^{2-} in neutral and basic medium are predominant factor for the adsorption of Cr(VI) onto PAZO nanocomposite.

At pH < 4, due to presence of excess of H^+ ions in the solution, the adsorbent surface becomes positively charged due to protonation and $HCrO_4^-$ form of Cr(VI) ions are dominant at lower pH [23], so strong electrostatic attraction between positively charged adsorbent surface and negatively charged $HCrO_4^-$ ions led to higher removal efficiency. However, as the pH increases, deprotonation of surface of the adsorbent was observed due to decrease in number of H^+ ions. So, lower adsorption capacity results due to less interaction between Cr(VI) ions and adsorbent surface at higher pH value. The point of zero charge of adsorbent surface is found to be 5.5.

3.2.2 Effect of contact time and initial metal ion concentration

The effect of retention time on removal efficiency of Cr(VI) was carried out by varying the contact time in the range of 10–300 min at three different metal ion concentrations 10, 50, and 100 mg L^{-1} at pH 2 at adsorbent dose of 0.04 g. The effect of contact time on PAZO for Cr(VI) removal is depicted in **Figure 7** indicating an initial increase in adsorption capacity with increase in time and attaining the equilibrium time at 120 min after that little change in adsorption capacity for Cr(VI) is seen which indicates that the system has already achieved equilibrium. No change in adsorption capacity after equilibrium reveals that the adsorption sites are completely occupied by metal ion. So, the equilibrium time 120 min was chosen as optimum time in subsequent experiments.

The initial metal ion concentration provides an important driving force to overcome all mass transfer resistance of metal ions between the aqueous and solid phases [24]. Three different concentrations 10, 50, and 100 mg L^{-1} of the metal ions were chosen to see the effect of initial metal ion concentration on adsorption capacity of PAZO. **Figure 7** also shows the effect of initial metal ion concentration in which by increasing Cr(VI) ions concentration the adsorption capacity also increases. The maximum adsorption capacity at 10, 50, and 100 mg L^{-1} was found to be 9.31, 25.11, and 31.89 mg g^{-1}, respectively, which might be due to the fact that increasing metal ion concentration increased the number of collision between the adsorbent and metal ion species, this leads to an increased metal ion uploading [25].
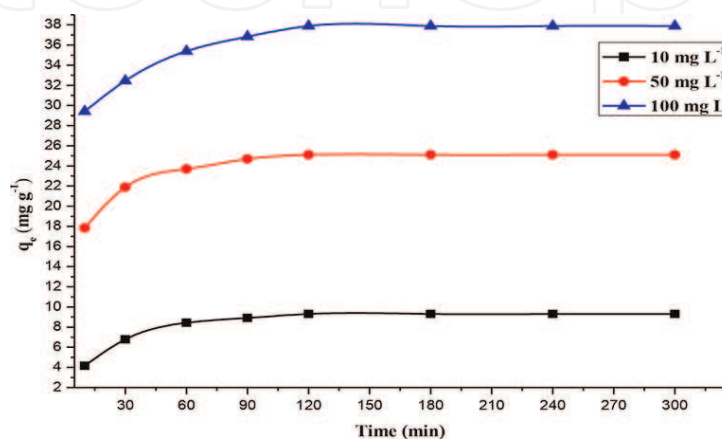

Figure 7.
Effect of contact time on adsorption of Cr(VI) on PAZO at 10, 50, and 100 mg L^{-1} initial metal ion concentrations.

3.2.3 Effect of adsorbent dose and temperature

The adsorption of metal ions in the solution is greatly affected by the dose of adsorbent used. A range of adsorbent dose from 0.01 to 0.07 g was used with 20 ml of 10, 50, and 100 mg L^{-1} of metal ion solution for 120 min to investigate the effect of dose on removal of Cr(VI), and the results are shown in **Figure 8**. It was found that the adsorption efficiency for Cr(VI) ion increases as the amount of adsorbent increase up to 0.04 g, but on further increasing the adsorbent dose, the adsorption capacity decreases. This trend can be explained as the adsorbent dose increases, the number of adsorbent particles also increases facilitating more active sites for adsorption but on further increase in adsorbent dose adsorption capacity decreases due to partial aggregation of adsorbent particles. So, 0.04 g was taken as optimum adsorbent dose for all the experiments.

The effect of temperature on adsorption of Cr(VI) was observed in the temperature range of 30–50°C (plot not given). It was observed that on increasing the temperature, the adsorption capacity also increases due to increase in diffusion rate of metal ions across the external boundary layer and within the pores of PAZO nanocomposite. Furthermore, at high temperature, the energy of the system also facilitated the binding of Cr(VI) on the surface of PAZO indicating the adsorption of Cr(VI) is controlled endothermic process. So, 50°C was selected as the optimum temperature for all the adsorption experiments.

3.3 Adsorption isotherms

The adsorption isotherms describe the effect of metal ion concentrations on the amount of metal ion adsorbed on the adsorbent surface leading to find the best equilibrium position in the adsorption process. In the present study, Langmuir [26], Freundlich [27] Dubinin-Radushkevich [28], and Temkin [29] models have been applied to the experimental data.

3.3.1 Langmuir isotherm

The Langmuir isotherm is used to describe the equilibrium between the surface of solid and the solution as a reversible chemical equilibrium. Langmuir isotherm model is valid for adsorption onto a surface containing a finite number of identical sites. The Langmuir treatment is based on the assumption that a maximum
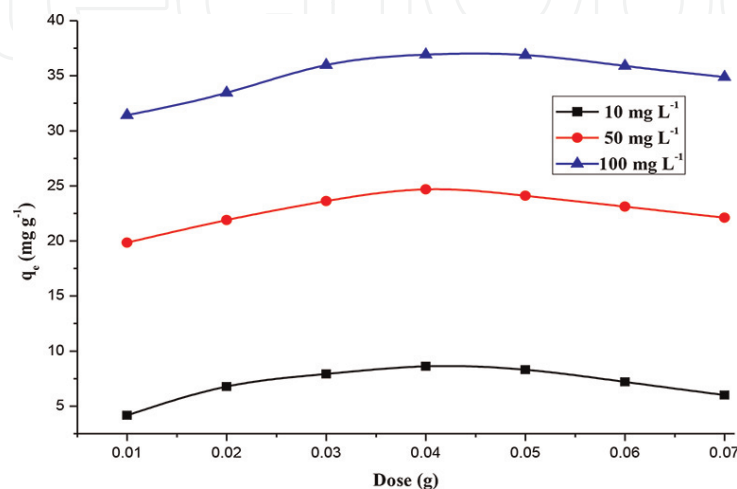

Figure 8.
Effect of adsorbent dose on adsorption of Cr(VI) on PAZO at 10, 50, and 100 mg L^{-1} initial metal ion concentrations.

adsorption corresponds to a saturated monolayer of solute molecules on the adsorbent surface which is represented as follows:

$$\frac{C_e}{q_e} = \frac{1}{q_m K_L} + \frac{C_e}{q_m} \qquad (2)$$

where q_m is maximum monolayer adsorption capacity of the adsorbent (mg g^{-1}) and K_L is the Langmuir constant (L mg^{-1}) related to the adsorption free energy. The q_m and K_L values are reported in **Table 1**. The essential feature of the Langmuir adsorption can be expressed by means of R_L, a dimensionless constant referred to as separation factor for predicting whether an adsorption system is favorable or unfavorable. R_L is calculated using equation

$$R_L = \frac{1}{1 + K_L C_o} \qquad (3)$$

where C_0 is the initial metal ion concentration (mg L^{-1}). The parameter R_L indicates the favorability of adsorption as follows:

- $R_L > 1$, unfavorable adsorption

- $0 < R_L > 1$, favorable adsorption

- $R_L = 0$, irreversible adsorption

- $R_L = 1$, linear adsorption

The linearized plot (**Figure 9**) of C_e/q_e versus C_e are obtained for Cr(VI). The Langmuir constants q_m and K_L can be determined from the slope and intercept of the linear line, respectively. As can be seen from **Table 1**, the maximum monolayer

Model	Parameters	Cr(VI)		
		30°C	40°C	50°C
Langmuir	qm (mg g^{-1})	120.92	134.22	139.47
	K$_L$ (L mg^{-1})	0.06	0.08	0.12
	R^2	0.99	0.99	0.99
Freundlich	n	1.18	1.22	1.35
	K$_L$ (mg g^{-1})	5.69	6.29	6.62
	R^2	0.98	0.98	0.98
D-R	qm (mg g^{-1})	59.05	62.18	68.70
	k$_{D-R}$ (mol^2 KJ^{-2})	$1.85 \times e^{-6}$	$1.47 \times e^{-6}$	$1.25 \times e^{-}$
	E (KJ mol^{-1})	10.48	11.71	12.65
	R^2	0.97	0.98	0.97
Temkin	A (L mg^{-1})	0.55	0.60	0.64
	b (J mol^{-1})	63.10	62.97	56.09
	R^2	0.98	0.98	0.98

Table 1.
Isotherm parameters for Cr(VI) removal by PAZO at 30, 40, and 50°C.

adsorption capacities (q_m) calculated by Langmuir model were found to be 120.92, 134.22, and 139.47 mg g^{-1} at 30, 40, and 50°C, respectively. The regression coefficient values calculated are 0.99, 0.99, and 0.99, respectively, which suggest that the Langmuir model is best fitted to the experimental data at all temperature ranges.

3.3.2 Freundlich isotherm

The Freundlich isotherm model is the earliest empirical equation based on the adsorption on reversible heterogeneous surfaces. The mathematical expression of the model is given as follows:

$$\ln q_e = \frac{1}{n}\ln C_e + \ln K_F \tag{4}$$

where K_F (mg g^{-1}) is approximately an indicator of the adsorption capacity, and $1/n$ is the adsorption intensity and an indicator for the favorability of adsorption. The values of $n > 1$ represent favorable adsorption condition. The linear plot (**Figure 10**) of $\ln q_e$ versus $\ln C_e$ gives slope of value $1/n$ and an intercept $\ln K_F$. When C_e equals unity, $\ln K_F$ is equal to $\ln q_e$. In the other case, when $1/n = 1$, the K_F value depends on the units in which q_e and C_e are expressed. A favorable adsorption tends to give Freundlich constant n value between 1 and 10. Larger value of n
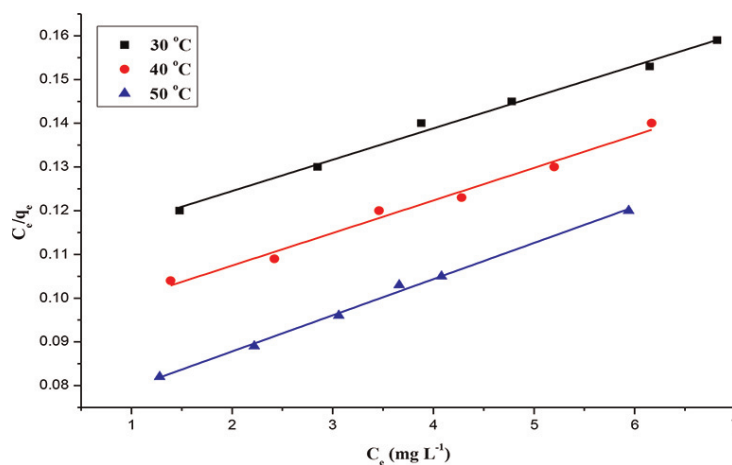

Figure 9.
Langmuir adsorption isotherm for Cr(VI) on PAZO at 30, 40, and 50°C (dose = 0.04 g and pH = 2).
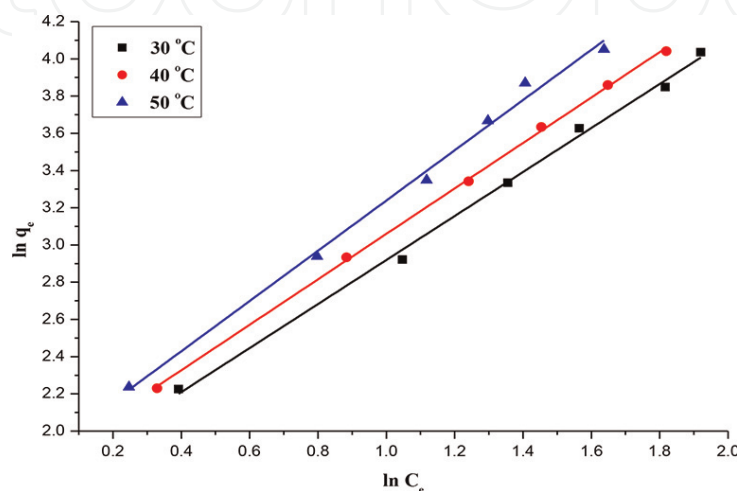

Figure 10.
Freundlich adsorption isotherm for Cr(VI) on PAZO at 30, 40, and 50°C (dose = 0.04 g and pH = 2).

(smaller value of $1/n$) implies strong interaction between sorbent and metal ions, while $1/n$ equal to 1 indicates linear adsorption leading to identical adsorption energies for all the sites. It can be observed from **Table 1** that for all the temperature ranges, the values of n is >1 and hence favorable adsorption.

3.3.3 Dubinin-Radushkevish (D-R) isotherm

The Dubinin-Radushkevish (D-R) isotherm can be used to describe adsorption on both homogeneous and heterogeneous surfaces. This isotherm can be described by the following equation:

$$\ln q_e = \ln q_m - k_{D-R}\varepsilon^2 \tag{5}$$

where q_m is the D-R monolayer capacity (mg g^{-1}) obtained by a plot between $\ln q_e$ and ε^2 (**Figure 11**), k_{D-R} is a constant related to the adsorption energy, and ε is Polanyi potential which is related to the equilibrium concentration as follows:

$$\varepsilon = RT\left(1 + \frac{1}{C_e}\right) \tag{6}$$

where R is the gas constant (8.314 Jmol^{-1} K^{-1}) and T is the absolute temperature (K). The constant k gives the mean free energy E of adsorption per molecule of the adsorbate when it is transferred to the surface of the solid from infinity in the solution and can be computed using the relationship:

$$E = \frac{1}{\sqrt{2k_{D-R}}} \tag{7}$$

The magnitude of E is useful for estimating the mechanism of the adsorption reaction. From **Table 1**, the maximum adsorption capacities for Cr(VI) calculated by D-R model at 30, 40, and 50°C was found to be 59.05, 62.18, and 68.70 mg g^{-1}, respectively. The mean free energy per molecule (E) was estimated to be 10.48, 11.71, and 12.65 KJ mol^{-1} at 30, 40, and 50°C, respectively, which confirms that the adsorption reaction follows chemisorption process. The values of D-R constant k_{D-R} were found to be 1.85×10^{-6}, 1.47×10^{-6}, and 1.25×10^{-6} for Cr(VI) at 30, 40, and 50°C, respectively.
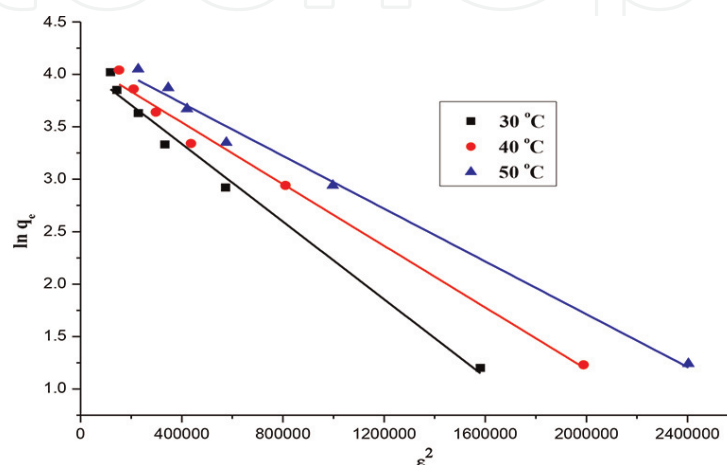

Figure 11.
D-R adsorption isotherm for Cr(VI) on PAZO at 30, 40, and 50°C (dose = 0.04 g and pH = 2).

3.3.4 Temkin isotherm

Temkin isotherm considers the effects of the heat of adsorption that decreases linearly with coverage of the adsorbate and adsorbent interactions. The Temkin isotherm has been used in the following forms:

$$q_e = B\ln A + B\ln C_e \tag{8}$$

$$B = \frac{RT}{b} \tag{9}$$

where R is gas constant 8.314 J mol^{-1} K^{-1}. T is absolute temperature (K), b is the Temkin constant related to the heat of adsorption (J mol^{-1}), and A is the equilibrium binding constant corresponding to the maximum binding energy (L g^{-1}). The liner plots (**Figure 12**) of q_e versus ln C_e enable to determine the constant A and B. The Temkin constant given in **Table 1** clearly suggests that the adsorption involves chemisorption and physisorption of the Cr(VI) rather than an ion exchange mechanism. The Temkin isotherm gives a satisfactory linear fit data with all the metal ions. The value of binding constant A given in **Table 1** as 0.55, 0.60, and 0.64 L mg^{-1} also support the high affinity of Cr(VI) toward adsorbent surface at high temperature.

3.4 Adsorption kinetics

Kinetics of the adsorption process is a vital parameter which provides essential information on the solute uptake rate and the reaction pathways. To determine the rate-determining step during the adsorption process, the kinetic data of heavy metals onto PAZO were simulated with the pseudo-first-order and pseudo-second-order, Elovich, and Webber-Morris intra-particle diffusion models.

3.4.1 Lagergren pseudo-first-order model

The pseudo-first-order kinetics model is based on the assumption that adsorption was controlled by diffusion steps [30] and the rate of adsorption is in direct proportion to the difference value of equilibrium adsorption capacity and the adsorption capacity at any time t. The linear equation for this model can be expressed by the following equation:

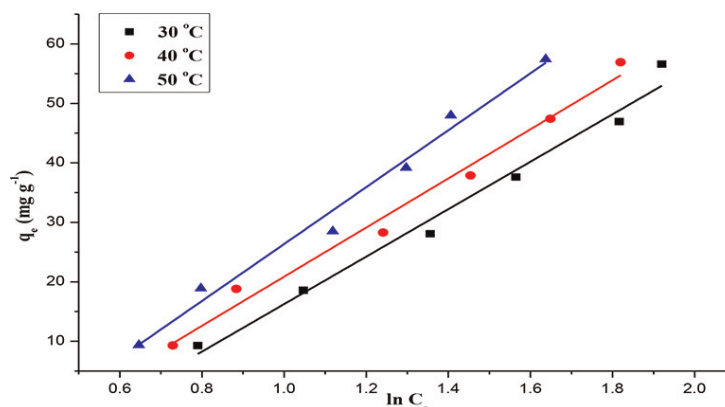$$\log{(q_e - q_t)} = \log q_e - \frac{k_1}{2.303}t \tag{10}$$

Figure 12.
Temkin adsorption isotherm for Cr(VI) on PAZO at 30, 40, and 50°C (dose = 0.04 g and pH = 2).

where k_1 is the pseudo-first-order rate constant (min^{-1}), q_e is the amount of heavy metal ions adsorbed at equilibrium (mg g^{-1}), and q_t is the amount of the adsorption at any time t (mg g^{-1}). Such an equation should yield a straight line, as given in **Figure 13**, with intercept equal to log q_e and slope equal to (k_1/2.303).

3.4.2 Pseudo-second order

The linear equation for pseudo-second-order kinetics [31] is given by the following equation:

$$\frac{t}{q_t} = \frac{1}{k_2 q e^2} + \frac{t}{q_e} \tag{11}$$

where k_2 is the pseudo-second-order rate constant (g mg^{-1} min^{-1}), q_e is the amount of heavy metal ions adsorbed at equilibrium (mg g^{-1}), and q_t is the amount of the adsorption at any time t (mg g^{-1}). The linear plot of pseudo-second-order model is given in **Figure 14**, from which constant k_2 and q_e can be calculated.
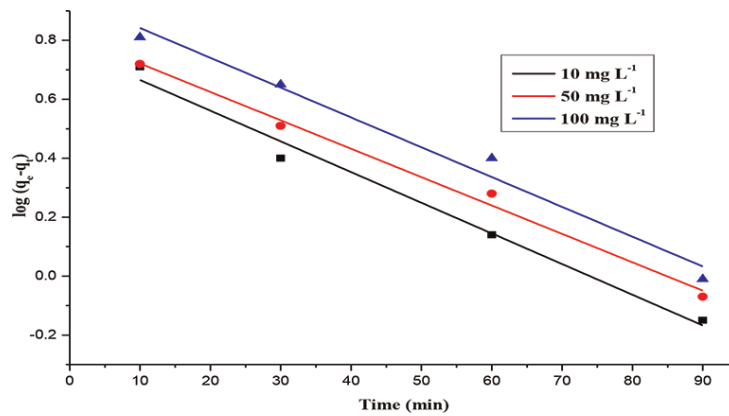

Figure 13.
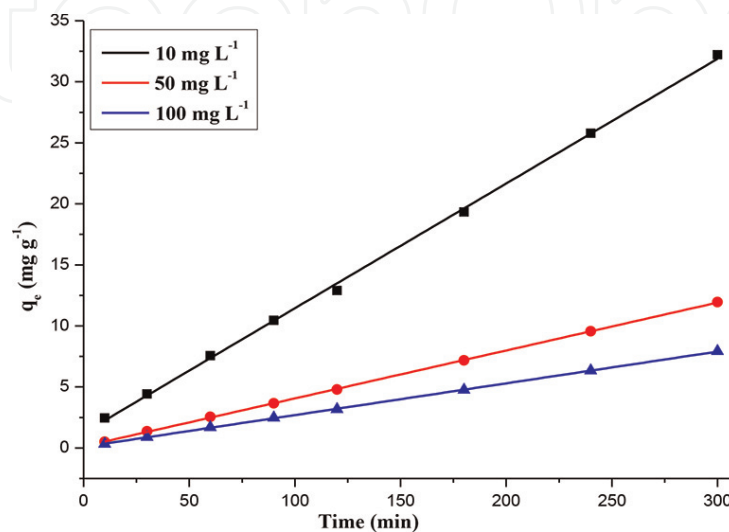*Pseudo-first-order model for Cr(VI) on PAZO at 10, 50, and 100 mg L^{-1} metal ion concentration (dose = 0.04 g and pH = 2).*

Figure 14.
Pseudo-second-order model for Cr(VI) on PAZO at 10, 50, and 100 mg L^{-1} metal ion concentration (dose = 0.04 g and pH = 2).

14

3.4.3 Elovich model

If the process is a chemisorption on highly heterogeneous sorbents, the sorption kinetics could be interpreted by Elovich equation [32] as follows:

$$q_t = \frac{1}{\beta}\ln t + \frac{1}{\beta}\ln(\alpha\beta) \qquad (12)$$

where α is the initial adsorption rate (mg g^{-1} min^{-1}), β is the adsorption constant (g mg^{-1}), and q_t is the adsorption capacity at any time t in mg g^{-1}. **Figure 15** shows a plot of linearization form of Elovich model. The slopes and intercepts of plots of q_t versus ln t were used to determine the constant β and the initial adsorption rate α.

3.4.4 Intra-particle diffusion model

When adsorbate transmits from solution into solid phase of absorbents, pore and intra-particle diffusion are often rate limiting in a batch reactor system. The intra-particle diffusion was explored by using the following equation suggested by Weber and Morris [33]:

$$q_t = K_{int}t^{1/2} + C \qquad (13)$$

where the parameter q_t is the amount adsorbed at time t (mg g^{-1}), K_{int} is the intra-particle diffusion equation constant (mg g^{-1} min$^{-1/2}$), and t is the time. According to the Weber-Morris model, the plot of q_t, against $t^{1/2}$, should give a straight line, when diffusion plays a role in the sorption rate, and should cross the origin if intra-particle diffusion is the rate-determining step. The intra-particle diffusion parameters can be calculated from the slope and intercept of the linear plot given in **Figure 16**.

The kinetic parameters obtained by the sorption of heavy metal ions on PAZO nanocomposite are summarized in **Table 2**. It is found that the correlation coefficients R^2 for the pseudo-second-order kinetic model are 0.99 for 10, 50, and 100 mg L^{-1} Cr(VI) concentration at 50°C, respectively, is higher than the correlation coefficient obtained for other models. Also, the q_{cal} values obtained through this model 9.79, 25.46, and 38.44 mg g^{-1} are much closer to q_{exp} values 9.31, 25.11, and 37.89 mg g^{-1} for 10, 50, and 100 mg L^{-1} Cr(VI) solution. The pseudo-second-order kinetic model assumes that the rate limiting step may be chemical adsorption,
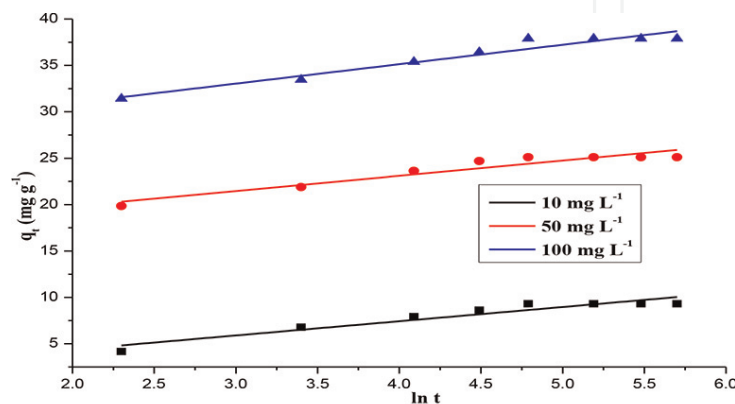

Figure 15.
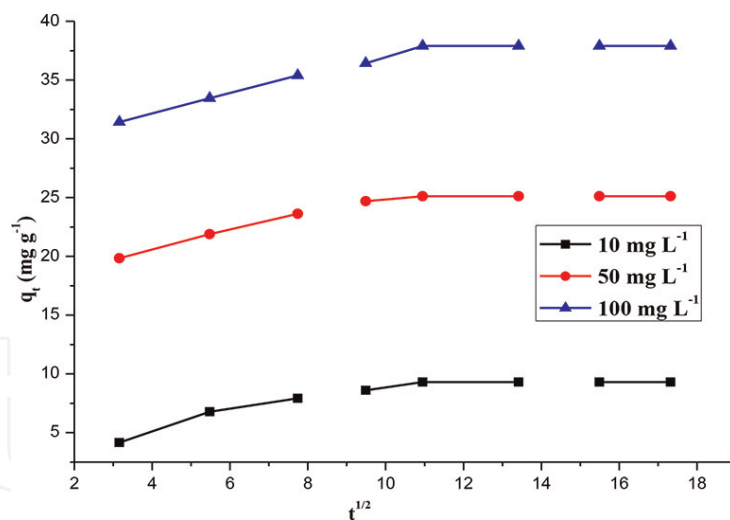*Elovich model for Cr(VI) on PAZO at 10, 50, and 100 mg L^{-1} metal ion concentration (dose = 0.04 g and pH = 2).*

Figure 16.
Intra-particle diffusion model for Cr(VI) on PAZO at 10, 50, and 100 mg L^{-1} metal ion concentration (dose = 0.04 g and pH = 2).

Model	Parameters	Cr(VI)		
		30°C	**40°C**	**50°C**
Pseudo-first-order	q_e (exp) (mg g^{-1})	9.31	25.11	37.89
	q_e (cal) (mg g^{-1})	5.88	6.57	8.77
	k_1 (min^{-1})	0.02	0.02	0.02
	R^2	0.97	0.98	0.97
Pseudo-second-order	q_e (exp) (mg g^{-1})	9.31	25.11	37.89
	q_e (cal) (mg g^{-1})	9.79	25.46	38.44
	k_2 (g mg^{-1} min^{-1})	2.19×10^{-3}	2.17×10^{-3}	2.18×10^{-3}
	R^2	0.99	0.99	0.99
Elovich	α (mg g^{-1} min^{-1})	3.59	3.88	7.57
	β (g mg^{-1})	0.65	0.61	0.48
	R^2	0.90	0.89	0.93
Intra-particle	K_{int} (mg g^{-1} min$^{-1/2}$)	0.32	0.35	0.45
	C (mg g^{-1})	4.75	20.21	31.30
	R^2	0.69	0.70	0.79

Table 2.
Kinetic parameters for Cr(VI) removal by PAZO at 50°C.

and the adsorption behavior of PAZO may involve valence forces through sharing of electrons between transition metal cations and the PAZO. Because of the fact that diffusion and adsorption are often experimentally inseparable, the uptake of metal ions onto nanocomposite may be a complicate process including diffusion, coordinating bond formation or chemical reaction simultaneously. However, from the results obtained, it can be observed that good fits to the experimental data are obtained with pseudo-second-order model for the metal ion at all concentration ranges at 50°C.

3.5 Adsorption thermodynamics

To substantiate our prediction about the endothermic nature of the adsorption process, thermodynamic parameters such as Gibbs free energy change ($\Delta G°$),

enthalpy change ($\Delta H°$), and entropy change ($\Delta S°$) were calculated using the Gibbs equation and the Van't Hoff equation, listed as follows:

$$\Delta G^o = -RT\ln K_c \tag{14}$$

$$\ln Kc = -\frac{\Delta H^o}{R} + \frac{\Delta S^o}{RT} \tag{15}$$

The gas constant R is defined by 8.3145 J mol^{-1} K^{-1}. K_c (C_{ad}/C_e) is the distribution coefficient; T is the temperature of the solution in Celsius. $\Delta G°$ and $\Delta S°$ were calculated from the slope and intercept of a plot of ln K_c as a function of $1/T$, as shown in **Figure 17**. The free energy change ($\Delta G°$) can be determined from the following equation:

$$\Delta G^o = \Delta H^o - T\Delta S^o \tag{16}$$

Thermodynamic parameters associated with the Cr(VI) adsorption by the nanocomposite are listed in **Table 3**. The positive value of $\Delta H°$ confirmed the endothermic nature of the adsorption process of Cr(VI) on PAZO. The values of $\Delta G°$ are all negative, and the negative value of $\Delta G°$ increases as the temperature increase from 30 to 50°C, which indicates that the Cr(VI) adsorption process of the nanocomposite is spontaneous and spontaneity increases with temperature [34]. The positive value of $\Delta S°$ revealed the increased randomness and an increase in the degrees of freedom at the adsorbent-solution interface during the immobilization of the heavy metal ions on the active sites of the adsorbent, which indicate the partial liberation of the salvation metal ions from solvent molecules before adsorption (liberation of water molecules from solvated-heavy metals), therefore, enabling commonness of randomness and spontaneity in the system.
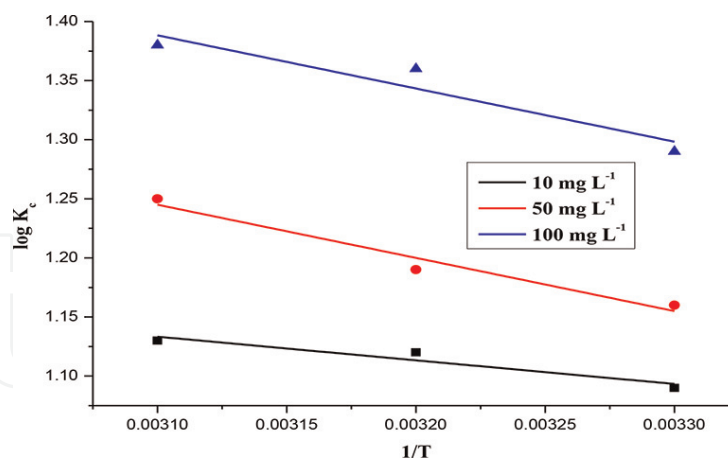

Figure 17.
Thermodynamic plot for removal of Cr(VI) on PAZO at 30, 40, and 50°C.

Concentration	ΔH° (KJ mol^{-1})	ΔS° (KJ mol^{-1} K^{-1})	ΔG° (KJ mol^{-1})		
			30°C	40°C	50°C
10 mg L^{-1}	1.66	0.014	−2.75	−2.89	−3.04
50 mg L^{-1}	3.74	0.021	−2.91	−3.13	−3.35
100 mg L^{-1}	3.74	0.023	−3.26	−3.50	−3.73

Table 3.
Thermodynamic parameters for Cr(VI) removal by PAZO.

4. Conclusion

In this chapter, polyaniline/zinc oxide nanocomposite was synthesized by oxidative free radical polymerization of aniline monomer in presence of zinc oxide nanoparticles. The material was characterized by various analytical techniques, such as FT-IR, XTD, TGA-DTG, SEM, and TEM. The nanocomposite material was further explored for the removal of Cr(VI) from aqueous solution. The effect of various adsorption parameters such as agitation time, solution pH, adsorbent dose, initial metal ion concentration, and temperature was observed and optimized by preliminary experiments. The adsorption of metal ions is highly pH-dependent and the maximum removal efficiencies and adsorption capacities of the selected metal ions were obtained at pH 2. The experimental data were tested using Langmuir, Freundlich, D-R and Temkin models and the data were best followed by Langmuir model. The maximum monolayer adsorption capacity was found to be 120.92 mg g^{-1} at 30°C, 134.22 mg g^{-1} at 40°C, and 139.47 mg g^{-1} at 50°C. All kinetic parameters suggest that the adsorption of metal ion by PAZO followed the second-order kinetics and chemisorption is the rate-determining step. The positive values of $\Delta H°$ and negative value of $\Delta G°$ indicate the adsorption process to be endothermic and spontaneous in nature.

Nomenclature

C_e	equilibrium adsorbate concentration in the solution (mg L^{-1})
C_0	initial adsorbate concentration in the solution (mg L^{-1})
C_{ab}	equilibrium concentration of adsorbate on the adsorbent surface (mg L^1)
q_e	amount of adsorbate adsorbed per unit mass of adsorbent at equilibrium or adsorption capacity (mg g^{-1})
m	amount of adsorbent (g)
DDW	double distilled water
AAS	atomic absorption spectrophotometer
FTIR	Fourier-transform infrared spectroscopy
SEM	scanning electron microscopy
EDX	energy dispersive X-ray analysis
TEM	transmission electron microscopy
XRD	X-ray diffraction
TGA	thermogravimetric analysis
q_e(exp)	adsorption capacity determined experimentally (mgg^{-1})
q_e(cal)	adsorption capacity calculated from model (mg g^{-1})
k_1	pseudo-first-order rate constant (min^{-1})
k_2	pseudo-second-order rate constant (g mg^{-1} min^{-1})
q_t	adsorption capacity at time t (mg g^{-1})
k_{id}	intra-particle diffusion rate constant (mg g^{-1} min$^{-1/2}$)
C	intra-particle constant related to thickness of boundary layer
A and B	Elovich constants (mg g^{-1})
K_c	equilibrium constant
b	Langmuir constant for energy of adsorption (L mg^{-1})
q_m	theoretical maximum monolayer adsorption capacity (mg g^{-1})
K_F	Freundlich isotherm constant (mg g^{-1})(L mg^{-1})$^{1/n}$
n	Freundlich exponent, dimensionless factor
K_T	Equilibrium binding constant (L mg^{-1})

B_T	Temkin constant related to heat of adsorption (J mol^{-1})
β	constant related to the adsorption energy (mol^2 kJ^{-2})
ε	Polanyi potential
E	mean free energy of adsorption (kJ mol^{-1})
ΔG	free energy change (kJ mol^{-1})
ΔH	enthalpy change (kJ mol^{-1})
ΔS	entropy change (kJ mol^{-1} K^{-1})
R	universal gas constant (J mol^{-1} K^{-1})
T	absolute temperature (K)
t	time (min)
V	volume of solution (liter)

Units

°C	degree celsius
K	kelvin
cm	centimeter
g	gram
mg	milligram
mg g^{-1}	milligram per gram
L	liter
ml	milliliter
mg L^{-1}	milligram per liter
µg L^{-1}	microgram per liter
M	molar
N	normality
h	hours
min	minute
J	joule
kJ	kilo joule
mol	mole
rpm	revolutions per minute
µg	microgram
Å	angstrom
nm	nanometer

Author details

Rais Ahmad
Environmental Research Laboratory, Department of Applied Chemistry, Aligarh
Muslim University, Aligarh, India

*Address all correspondence to: rais45@rediffmail.com

IntechOpen

References

[1] Li H, Li J, Chi Z, Ke W. Kinetic and equilibrium studies of Cr (III) removal from aqueous solution by IRN-77 cation-exchange resin. Procedia Environmental Sciences. 2012;**16**:646-655

[2] Chen S, Yue Q, Gao B, Xu X. Equilibrium and kinetic adsorption study of the adsorptive removal of Cr (VI) using modified wheat residue. Journal of Colloid and Interface Science. 2010;**349**:256-264

[3] Jain M, Garg VK, Kadirvelu K. Adsorption of hexavalent chromium from aqueous medium onto carbonaceous adsorbents prepared from waste biomass. Journal of Environmental Management. 2010;**91**: 949-957

[4] Kocaoba S, Akcin G. Removal and recovery of chromium and chromium speciation with MINTEQA2. Talanta. 2002;**57**:23-30

[5] Pang Y, Zeng G, Tanga L, Zhang Y, Liu Y, Lei X, et al. Preparation and application of stability enhanced magnetic nanoparticles for rapid removal of Cr (VI). Chemical Engineering Journal. 2011;**175**:222-227

[6] AL-Othman ZA, Ali R, Naushad M. Hexavalent chromium removal from aqueous medium by activated carbon prepared from peanut shell: Adsorption kinetics, equilibrium and thermodynamic studies. Chemical Engineering Journal. 2012;**184**:238-247

[7] AL-Othman ZA, Ali R, Naushad M. Kinetic, equilibrium isotherm and thermodynamic studies of Cr (VI) adsorption onto low-cost adsorbent developed from peanut shell activated with phosphoric acid. Environmental Science and Pollution Research. 2013; **20**:3351-3365

[8] Shin K, Hong J, Jang J. Heavy metal ion adsorption behaviour in nitrogen-doped magnetic carbon nanoparticles: Isotherms and kinetic study. Journal of Hazardous Materials. 2011;**190**:36-44

[9] Noreen S, Bhatti HN, Nausheen S, Sadaf S, Ashfaq M. Batch and fixed bed adsorption study for the removal of Drimarine Black CL-B dye from aqueous solution using a lignocellulosic waste: A cost effective adsorbent. Industrial Crops and Products. 2013;**50**: 568-579

[10] Noreen S, Bhatti HN, Nausheen S, Zahid M, Asim S. Biosorption of Drimarine Blue HF-RL using raw, pretreated and immobilized peanut hulls. Desalination and Water Treatment. 2014;**52**:7339-7353

[11] Tofighy MA, Mohammadi T. Adsorption of divalent heavy metal ions from water using carbon nanotube sheets. Journal of Hazardous Materials. 2011;**185**:140-147

[12] Gupta VK, Jain R, Saleh TA, Nayak A, Malathi S, Agarwal S. Equilibrium and thermodynamic studies on the removal and recovery of Safranine-T dye from industrial effluents. Separation Science and Technology. 2011;**46**: 839-846

[13] Shahat A, Awual MR, Khaleque MA, Alam MZ, Naushad M, Chowdhury AMS. Large-pore diameter nano-adsorbent and its application for rapid lead (II) detection and removal from aqueous media. Chemical Engineering Journal. 2015;**273**:286-295

[14] Nausheen S, Bhatti HN, Furrukh Z, Sadaf S, Noreen S. Adsorptive removal of Drimarine Red HF-3D dye from aqueous solution using low-cost agricultural waste: Batch and column study. Chemistry and Ecology. 2015;**30**: 376-392

[15] Ahmad R, Kumar R. Conducting polyaniline/iron oxide composite:

A novel adsorbent for the removal of amido black 10B. Journal of Chemical & Engineering Data. 2010;**55**:3489-3493

[16] Kanwal F, Rehman R, Anwar J, Saeed M. Batchwise removal of chromium (VI) by adsorption on novel synthesized polyaniline composites with various brans and isothermal modelling of equilibrium data. Journal of the Chemical Society of Pakistan. 2012;**34**:1134-1139

[17] Zhu J, He H, Zhu L, Wen X, Deng F. Characterization of organic phases in them interlayer of montmorillonite using FTIR and 13C NMR. Journal of Colloid and Interface Science. 2005;**286**:239-244

[18] Khan TA, Nazir M, Ali I, Kumar A. Removal of chromium(VI) from aqueous solution using guar gum-nano zinc oxide biocomposite adsorbent. Arabian Journal of Chemistry. 2013

[19] Vigneshwaran N, Kumar S, Kathe AA, Varadarajan PV, Prasad V. Functional finishing of cotton fabrics using zinc oxide-soluble starch nanocomposites. Nanotechnology. 2006;**17**:5087-5095

[20] Sedaghat S. Synthesis and characterization of new biocompatible copolymer: Chitosan-graft polyaniline. International Nano Letters. 2014;**4**:1-6

[21] Shi L, Wang X, Lu L, Yang X, Wu X. Preparation of TiO_2/polyaniline nanocomposite from a lyotropic liquid crystalline solution. Synthetic Metals. 2009;**159**:2525-2529

[22] Sharma AL, Saxena V, Annopoorni S, Malhotra BD. Synthesis and characterization of a copolymer: Poly (aniline-co-fluoroaniline). Journal of Applied Polymer Science. 2001;**81**:1460-1466

[23] Yavuz AG, Dincturk-Atalay E, Uygun A, Gode F, Aslan E. A

comparison study of adsorption of Cr (VI) from aqueous solutions onto alkyl-substituted polyaniline/chitosan composites. Desalination. 2011;**279**:325-331

[24] Ajouyed O, Hurel C, Ammari M, Allal LB, Marmier N. Sorption of Cr (VI) onto natural iron and aluminum (oxy) hydroxides: Effects of pH, ionic strength and initial concentration. Journal of Hazardous Materials. 2010;**174**:616-622

[25] Monier M, Ayad DM, Sarhan AA. Adsorption of Cu (II), Hg (II), and Ni (II) ions by modified natural wool chelating fibers. Journal of Hazardous Materials. 2010;**176**:348-355

[26] Langmuir I. Adsorption of gaseous on plane surface of glass, mica and platinum. Journal of the American Chemical Society. 1918;**40**:1361-1403

[27] Freundlich HMF. Over the adsorption in solution. Zeitschrift für Physikalische Chemie. 1906;**57**:385-470

[28] Dubinin MM. The potential theory of adsorption of gases and vapours for adsorbents with energetically non-uniform surface. Chemical Reviews. 1960;**60**:235-266

[29] Temkin MJ, Pyzhev V. Kinetics of ammonia synthesis on promoted iron catalysts. Acta Physicochimica. 1940;**12**:217-222

[30] Lagergren S. About the theory of so-called adsorption of soluble substances. The Hand. 1898;**24**:1-39

[31] Ho YS. Review of second-order models for adsorption systems. Journal of Hazardous Materials. 2006;**136**:681-689

[32] El-Ashtoukhya E-SZ, Amina NK, Abdelwahab O. Removal of lead (II) and copper (II) from aqueous solution using

pomegranate peel as a new adsorbent. Desalination. 2008;**223**:162-173

[33] Weber WJ Jr, Morris JC. Kinetics of adsorption on carbon from solution. Journal of the Sanitary Engineering Division: American Society of Civil Engineers. 1963;**89**:31-59

[34] Ahmet Sari A, Mendil D, Tuzen M, Soylak M. Biosorption of palladium(II) from aqueous solution by moss (*Racomitrium lanuginosum*) biomass: Equilibrium, kinetic and thermodynamic studies. Journal of Hazardous Materials. 2009;**162**:874-879